

UNCLASSIFIED

Defense Technical Information Center
Compilation Part Notice

ADP014104

TITLE: Flow Field and Sound Radiation of a Mach 0.9 Jet Computed by
LES

DISTRIBUTION: Approved for public release, distribution unlimited
Availability: Hard copy only.

This paper is part of the following report:

TITLE: Aging Mechanisms and Control. Symposium Part A -
Developments in Computational Aero- and Hydro-Acoustics. Symposium
Part B - Monitoring and Management of Gas Turbine Fleets for Extended
Life and Reduced Costs [Les mecanismes vieillissants et le controle]
[Symposium Partie A - Developpements dans le domaine de
l'aeroacoustique et l'hydroacoustique numeriques] [Symposium Partie B ...

To order the complete compilation report, use: ADA415749

The component part is provided here to allow users access to individually authored sections
of proceedings, annals, symposia, etc. However, the component should be considered within
the context of the overall compilation report and not as a stand-alone technical report.

The following component part numbers comprise the compilation report:

ADP014092 thru ADP014141

UNCLASSIFIED

Flow Field and Sound Radiation of a Mach 0.9 Jet Computed by LES

Christophe Bogey, Christophe Bailly and Daniel Juvé

Laboratoire de Mécanique des Fluides et d'Acoustique

Ecole Centrale de Lyon & UMR CNRS 5509

BP 163, 69131 Ecully Cedex, France

1. Introduction

Spectacular improvements in jet noise prediction have been performed in the last decade, due to the progress in numerical simulations. Noting that hybrid approaches based on acoustic analogies present difficulties related to the modelling of source terms and to the formulation of a wave operator accounting for acoustic-flow interactions, methods for computing the sound directly from the resolution of the unsteady compressible Navier-Stokes equations have been developed. The objective of this approach is to determine both the flow field and the acoustic waves in the same calculation. In this way, the computed sound field is *a priori* exact because no acoustic model is used. It will also permit to investigate the sound generation mechanisms since all flow and acoustic quantities are provided by the computation. However, serious numerical issues¹ must be taken into account in this direct acoustic approach, owing to the great disparity of levels and length scales between the flow and the acoustic field. To overcome these difficulties, numerical techniques specific to Computational AeroAcoustics (CAA), suited to the behaviour of acoustic waves, have been proposed, such as non dispersive and non dissipative numerical schemes, or non-reflective boundary conditions. To make direct aeroacoustic calculations, the challenge is then to combine these CAA techniques with one of the methods used to solve the Navier-Stokes equations.

The three classical approaches commonly used to solve these flow equations have thus been experimented for aeroacoustic simulations: Direct Numerical Simulations (DNS) consisting in computing all turbulent scales, Large Eddy Simulations (LES) where only larger scales are calculated whereas the effects of unresolved ones are modeled via a subgrid scale model, and the unsteady Reynolds Averaged Navier-Stokes equations (RANS) using turbulence closures. Among the first three-dimensional applications performed in the last five years, we can put forward the DNS of Freund *et al.*^{2,3} of the noise radiated by supersonic and subsonic circular jets, the LES of Morris *et al.*⁴ of the radiation of a supersonic rectangular jet, and the study of screech tones generation in a round jet using unsteady RANS by Shen & Tam.⁵

The use of LES is important because it can theoretically be applied to high Reynolds number flows unlike DNS which is restricted to very low Reynolds number flows. Therefore, in the present study, a Large Eddy Simulation of a three-dimensional circular jet with a Mach number of 0.9 and a Reynolds number of 65000 is performed, carrying on earlier preliminary works.⁶ The motivation is to show the feasibility of the the direct computation by LES of the sound generated by a subsonic flow. For this, CAA numerical methods are used in the simulation. The validation of the computation is then carried out by comparing systematically both flow properties and the radiated sound field with experimental data.

This paper is organized as follows. Numerical procedure, characteristics of the jet and parameters of the simulation are presented in section 2. The flow development is briefly shown in section 3, by studying the mean flow and the turbulent intensities. The radiated acoustic field is then investigated in section 4. Finally, concluding remarks are given in section 5.

2. Numerical simulation

2.1 Numerical procedure

The full three-dimensional Navier-Stokes equations written in a conservative form are solved. The numerical algorithm is low-dispersive and low-dissipative to compute directly the sound waves with accuracy, and has been successfully used in an earlier study on a two-dimensional mixing layer.⁶ It combines the Dispersion-Relation-Preserving (DRP) finite-difference scheme of Tam & Webb⁷ for space discretization with a four-step Runge-Kutta scheme for time integration. A selective damping¹ is also applied to filter out numerical oscillations, typically grid-to-grid waves, which are not computed properly by the algorithm, and to ensure numerical stability. The mesh is Cartesian and non uniform, to use different discretizations in the flow field and in the acoustic far-field.

The resolution of the full Navier-Stokes equations without modelling, by Direct Numerical Simulations (DNS), requires the calculation of all turbulent scales and is intrinsically restricted to low Reynolds number flows. To simulate flows at higher Reynolds number, Large Eddy Simulation (LES) can be performed by computing only the larger scales and by taking into account the effects of unresolved ones through a subgrid scale model. In the present study, a turbulent viscosity is classically implemented to provide the dissipation of the unresolved scales. Various models have been developed to give an evaluation of the turbulent viscosity from the resolved scales. To keep the problem as simple as possible for aerodynamics, we choose the Smagorinsky model.⁸

2.2 Boundary Conditions

In acoustic simulations, boundary conditions must minimize the magnitude of acoustic waves reflected when fluctuations leave out the computational domain. In this study, a formulation⁹ derived from the behaviour of sound waves in the acoustic far-field is used. It is the extension of Tam & Dong¹⁰ conditions for a three-dimensional geometry. Two conditions are applied: a

radiation condition for the inflow and for the lateral boundaries of the computational domain where only acoustic fluctuations propagate, and an outflow condition for the outflow where vortical and entropic disturbances are also convected by the flow.

The efficiency of the boundary conditions has been estimated using test cases.¹¹ The exit of vortical structures generates low-amplitude spurious waves, which are however not negligible with respect to the physical sound field characterized by very small amplitudes. Therefore a sponge zone is implemented in the outflow direction to dissipate flow fluctuations before they reach the outflow boundary, and also to filter out possible reflected waves. It is based on the combination of grid stretching with an artificial damping.⁶

2.3 Flow Parameters

The inflow longitudinal velocity $u(r)$ of the jet is given by the following hyperbolic-tangent profile

$$u(r) = \frac{U_j}{2} + \frac{U_j}{2} \tanh\left(\frac{r_0 - r}{2\delta_\theta}\right)$$

where U_j is the inflow centerline velocity, δ_θ the initial momentum thickness of the shear layer, and r_0 the jet radius. The fluid surrounding the jet is initially at rest.

The jet Mach number is $M_j = 0.9$. This choice is justified by the amount of experimental studies available in the literature, providing both aerodynamic results,¹² and acoustic results.¹³⁻¹⁵ This Mach number implies also a high convection speed of turbulent structures, which reduces computation time. We can notice that the first simulation of a subsonic jet to determine directly its radiated field, a DNS carried out by Freund,³ involves a Mach number 0.9, Reynolds number 3600 jet. In the present simulation, the jet Reynolds number is $Re_D = U_j \times D/\nu = 65000$. It is higher than Reynolds numbers reachable by DNS, but still lower than values of practical interest. The ratio between the initial jet radius and the initial momentum thickness of the shear layer δ_θ/r_0 is also an important parameter, because the laminar-turbulent transition depends on it. In this study, $\delta_\theta/r_0 = 0.05$, and the development of vortical structures in the shear zones is possible.

Finally, to obtain the natural flow development, the jet is forced by adding random velocity fluctuations into the inflow. These fluctuations are solenoidal to minimize the generation of spurious acoustic waves by the excitation. They are introduced only in the shear layers, which are the unstable region of the jet. In these shear zones, turbulent intensities generated by the forcing are around 3%, which is similar to intensities measured near jet nozzle exits.

2.4 Numerical specifications

The computational domain, discretized by a grid of $255 \times 187 \times 127$ points, is defined by $0 \leq x/r_0 \leq 30$, $-5 \leq y/r_0 \leq 25$ and $-5 \leq z/r_0 \leq 5$ in the three coordinate directions. Radially, points are clustered in the jet with 26 points in the radius. The mesh spacing is minimum around $r = r_0$ with $\Delta_0 = \delta_\theta/1.6$, and increases outside the jet to reach $\Delta y_{max} = 0.4r_0$ in far-field. In the flow direction, the mesh spacing is constant up to $x = 20r_0$, with $\Delta x = 3\Delta_0$. Then, meshes are

stretched, to obtain $\Delta x_{max} = 0.54r_0$, to form a sponge zone. An artificial damping is moreover applied in this zone, in the flow region only. In this way, the physical part of the computational domain extends up to $x = 20r_0$ for the flow field, and up to $x = 30r_0$ for the acoustic field.

The time step is given by $\Delta t = 0.7\Delta_0/c_0$. The simulation runs for 30000 iterations, the calculation of statistical means being performed only after 5000 iterations. Consequently, the simulation time corresponds to $22 \times Lx/c_0$, where $Lx = 30r_0$. The computation is 15 hours long on a Nec SX-5, with a CPU time of $0.3\mu s$ per grid point and per iteration. More details of the simulation can be found in earlier papers.^{9,11}

3. Flow Field

3.1 Flow Development

Figure 1 displays the vorticity fields provided by the simulation. The longitudinal vorticity field ω_{xy} shows that, initially, vortical structures are generated and grow in the shear layers. The shear zones of the jet interact around $x \simeq 10r_0$, indicating the end of the potential core, which is consistent with experimental observations.¹² A developed turbulence is found downstream, illustrated by the transverse vorticity field ω_{yz} , and characterized by a typical three-dimensional mixing. Finally, flow fluctuations are dissipated by the sponge zone for $x > 20r_0$.

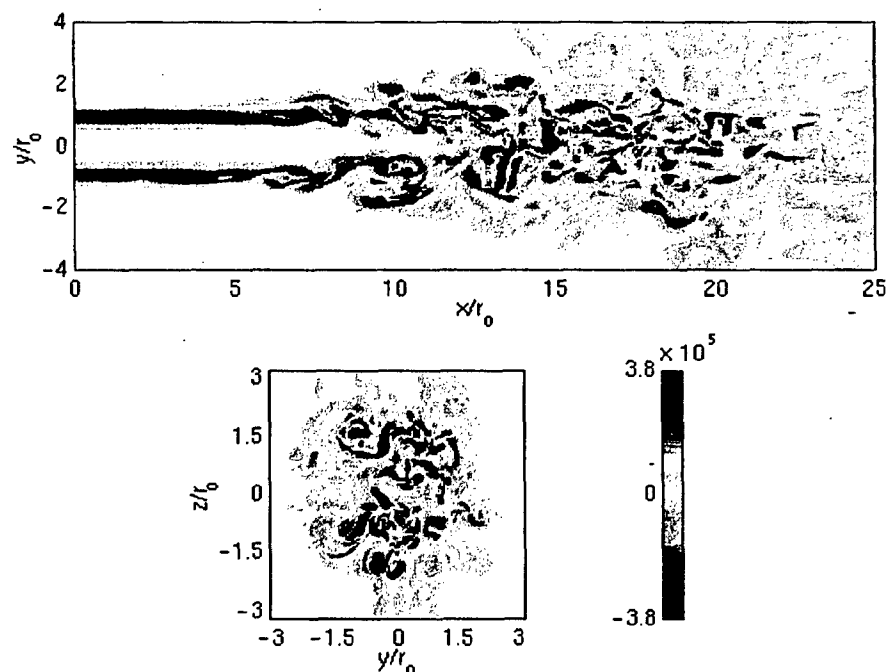


Figure 1: Snapshots of the vorticity field. Upper picture, ω_{xy} in the $x - y$ plane at $z = 0$; bottom picture, ω_{yz} in the $y - z$ plane at $x = 12r_0$. Levels are given in s^{-1} .

3.2 Mean Flow Properties

The characteristics of the jet mean flow calculated from the simulation are presented in Figures 2. First, Figure 2(a) displays the longitudinal evolution of the inverse of the mean centerline velocity normalized by the inflow velocity U_j . Its value is 1 in the potential core, and grows linearly afterwards so that we can write $U_c/U_j = B \times D/(x - x_0)$ where $x_0 = 0$ is the virtual origin, and $B = 5.5$. This value is consistent with measurements of Wygnanski & Fiedler,¹⁶ Panchapakesan & Lumley¹⁷ and Hussein *et al.*,¹⁸ as well as DNS result of Boersma *et al.*,¹⁹ reported in Table 1.

Re_D	B	A	Reference
8.6×10^4	5.4	0.086	Wygnanski* <i>et al.</i> ¹⁶
1.1×10^4	6.1	0.096	Panchapakesan* <i>et al.</i> ¹⁷
9.5×10^4	5.8	0.094	Hussein* <i>et al.</i> ¹⁸
2.4×10^3	5.9	0.095	Boersma** <i>et al.</i> ¹⁹
6.5×10^4	5.5	0.096	Present simulation

Table 1: Mean flow parameters obtained from experiments*, DNS**, and present simulation.

Second, Figure 2(b) presents the longitudinal evolution of the jet half-width $\delta_{1/2}$ normalized with the radius r_0 . Its value is fairly 1 up for $x < 6r_0$ where no large vortical structure is visible. Afterwards, in the turbulent region, the jet spreads linearly as $\delta_{1/2} = A \times (x - x_0)$ where $A = 0.096$, that is in agreement with data of Table 1.

Third, Figure 2(c) shows the longitudinal evolution of the flow rate. It grows regularly, indicating that the entrainment of the surrounding fluid occurs from the inflow of the computational domain. As deduced from the x^{-1} decay of the centerline velocity and from the linear spreading, a linear growth is found after the potential core, as $Q/Q_0 = C \times (x - x_0)/D$ where Q_0 is the initial flow rate and $C = 0.32$. This corresponds exactly to the measurement of Ricou & Spalding.²⁰

Finally, radial profiles of the mean longitudinal velocity normalized by the centerline velocity U_c are plotted in Figure 2(d) as function of the nondimensional coordinate $y/(x - x_0)$, for five locations between $x = 15r_0$ and $x = 20r_0$. The spreading rate A is the half-width of the profiles which are superimposed. This confirms the self-similarity in the turbulent jet suggested by the previous longitudinal evolutions.

3.3 Turbulent Intensities

Intensities of flow perturbations in the jet are investigated. They are calculated in the $x - y$ plane at $z = 0$ using velocity fluctuations u' , v' et w' and normalized with the local mean centerline longitudinal velocity U_c . They are given by the following expressions: $\sigma_{uu} = \sqrt{u'^2}/U_c$, $\sigma_{vv} = \sqrt{v'^2}/U_c$, $\sigma_{ww} = \sqrt{w'^2}/U_c$, and $\sigma_{uv} = \sqrt{|u'v'|}/U_c$.

Radial profiles of the turbulent intensities are shown in Figures 3 for five locations between $x = 15r_0$ and $x = 20r_0$, as function of the nondimensional coordinate $y/(x - x_0)$. Profiles are well superimposed, that is in agreement with the self-similarity in a fully turbulent jet. The mean

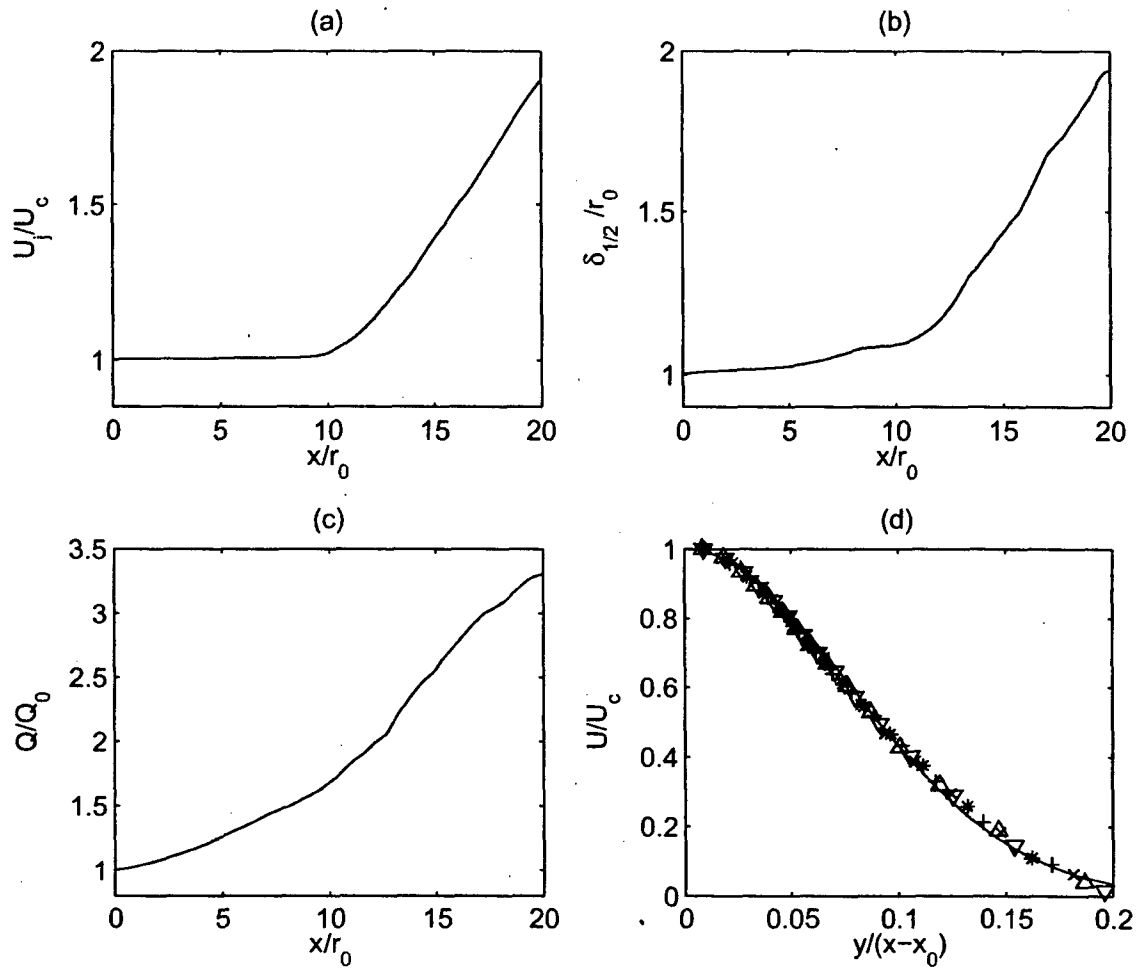


Figure 2: Longitudinal evolution of: (a), the inverse of the mean centerline velocity normalized with the inflow velocity U_j/U_c ; (b), the half-width of the jet normalized with the jet radius δ_{12}/r_0 ; (c), the mean flow rate normalized with the inflow rate Q/Q_0 . (d), Radial profiles of the mean longitudinal velocity normalized by the local centerline velocity U/U_c : \times , at $x = 15.8r_0$; $+$, at $x = 16.8r_0$; $*$, at $x = 17.7r_0$; ∇ , at $x = 18.6r_0$; Δ , at $x = 19.6r_0$. —, approximation with a Gaussian profile.

profiles calculated between $x = 15r_0$ and $x = 20r_0$ are also plotted as solid lines. They are very close to measurements, and stand between two experimental profiles provided by Panchapakesan & Lumley¹⁷ and by Hussein *et al.*¹⁸ respectively.

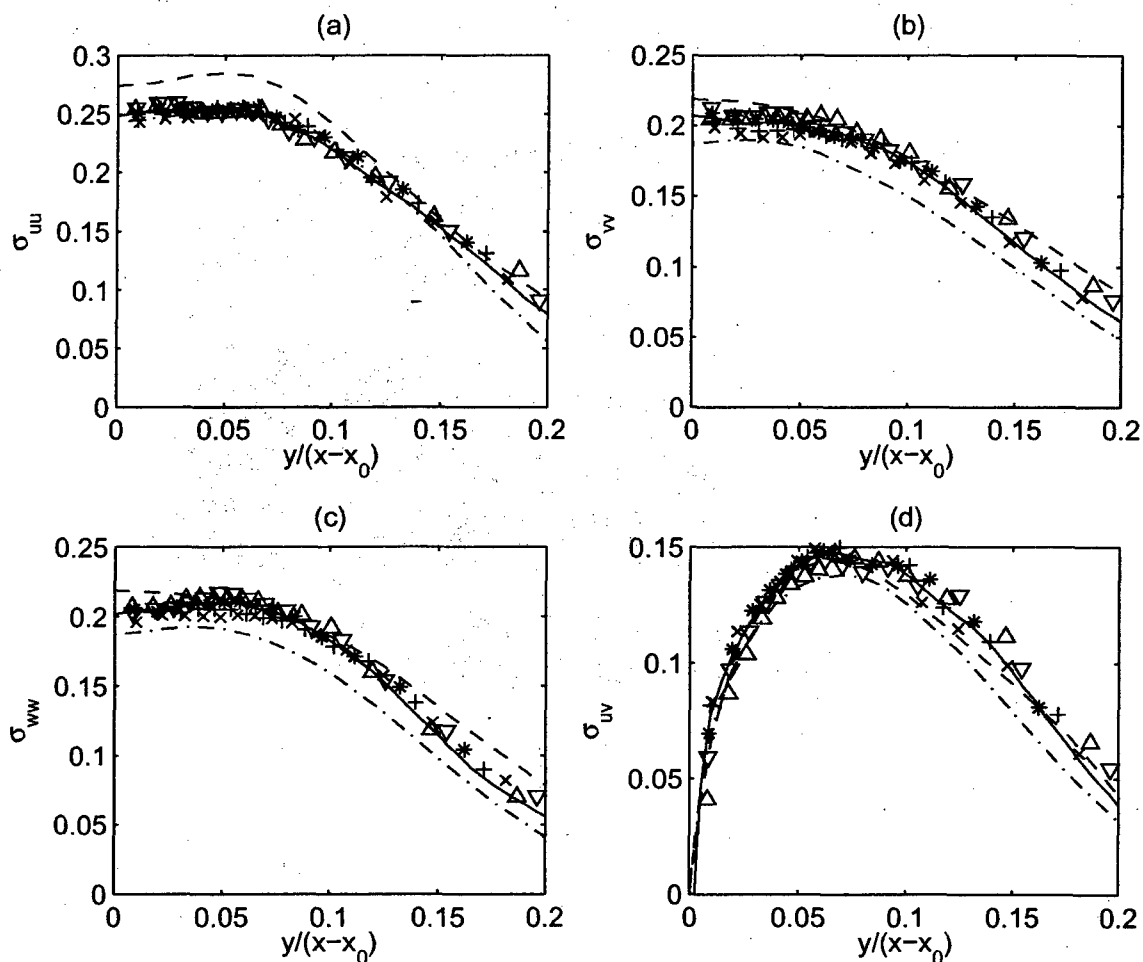


Figure 3: Radial profiles of the turbulent intensities: (a), σ_{uu} ; (b), σ_{vv} ; (c), σ_{wv} . \times , at $x = 15.8r_0$; $+$, at $x = 16.8r_0$; $*$, at $x = 17.7r_0$; ∇ , at $x = 18.6r_0$; \triangle , at $x = 19.6r_0$. —, mean profiles calculated from $x = 15r_0$ to $x = 20r_0$; - - - , experimental profiles obtained by Panchapakesan & Lumley¹⁷; - · - , experimental profiles obtained by Hussein, Capp & George.¹⁸

4. Sound Radiation

4.1 Dilatation field

Figure 4 displays the dilatation field $\Theta = \nabla \cdot \mathbf{u}$ provided directly by the simulation. Outside the flow region where the mean flow is negligible, dilatation is proportional to the time derivative of the acoustic pressure via the relation $\Theta = -(1/\rho_0 c_0^2) \partial p / \partial t$.

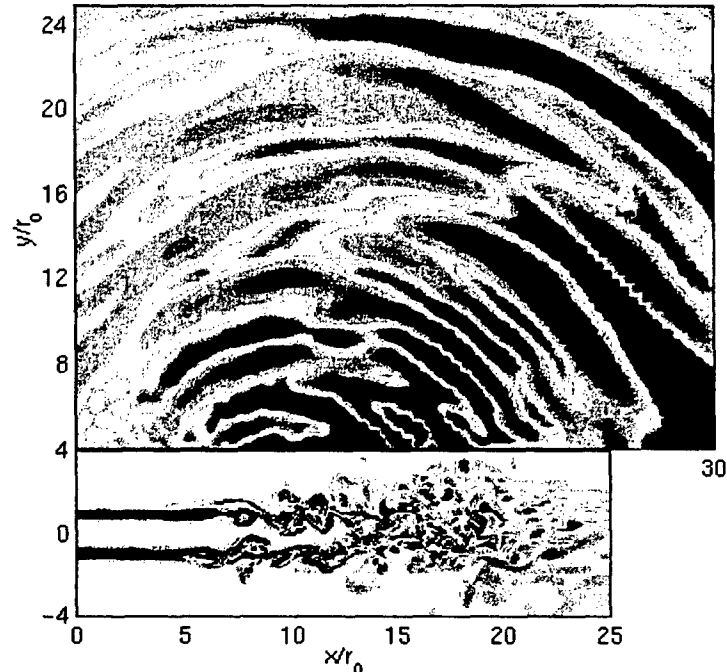


Figure 4: Snapshot of the dilatation field $\Theta = \nabla \cdot \mathbf{u}$ in the acoustic region, and of the vorticity field ω_{xy} in the aerodynamic region, in the $x - y$ plane at $z = 0$. The dilatation color scale is defined for levels from -90 à 90 s^{-1} , the vorticity scale is the same as in Figure 1.

This figure demonstrates that the dilatation field is not contaminated by spurious waves generated by the inflow excitation or reflected by the boundary conditions. Moreover, wave fronts are mainly coming from an origin located around $x \simeq 10r_0$, in the region where the mixing layers are merging, showing that predominant sound sources are located in the vicinity of the end of the potential core. This agrees both with the results of the recent DNS performed by Freund³ and with the measurements of Chu & Kaplan²¹ and Juvé *et al.*²² using various source localization techniques. The computed radiated field is also more pronounced in the downstream direction according to experimental directivities.

4.2 Pressure field spectra

To characterize the computed acoustic field, sound pressure spectra are calculated in far field. They are transposed at a distance of $60r_0$ from the inflow using the r^{-1} decay of acoustic waves

from the sound sources located at $x = 10r_0$ to the recording points.

Figures 5(a) and (b) show the spectra found for angles of 30° and of 90° from the jet axis for Strouhal numbers $St > 0.15$. Levels are more than 10 dB higher for $\theta = 30^\circ$ than for $\theta = 90^\circ$. Shapes are also different: for $\theta = 30^\circ$, the spectrum is dominated by low frequency components with a peak found around $St \simeq 0.2$, whereas for $\theta = 90^\circ$, the spectrum is larger with a preferred band of $0.2 < St < 0.5$ and a peak evaluated around $St \simeq 0.3$. This behaviour corresponds to experimental results,^{14,22} and the classical interpretation is that, at low angles, the noise is mainly generated by the large scales, whereas at higher angles the fine-scale turbulence is responsible for a great part of the noise.

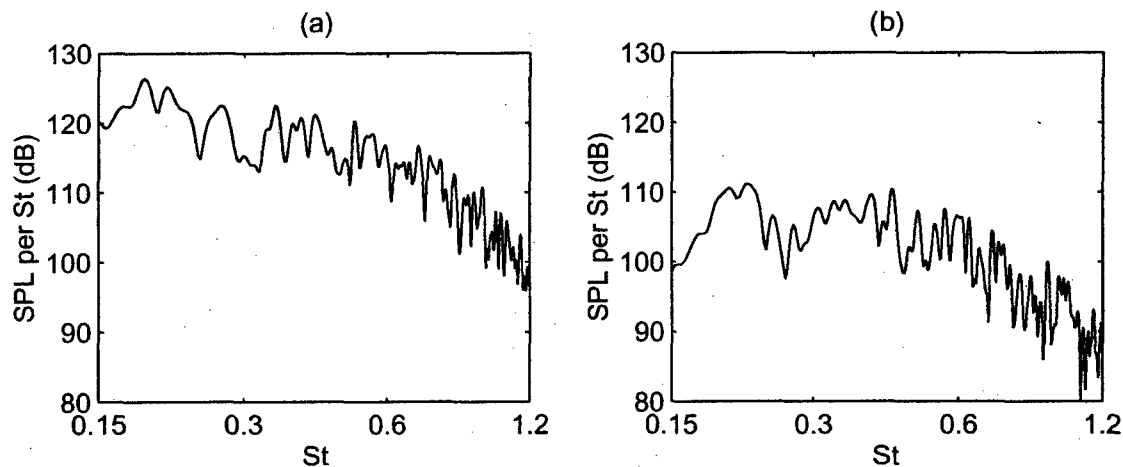


Figure 5: Sound pressure level as function of Strouhal number $St = fD/U_j$, at $60r_0$ from the jet nozzle, for an angle of: (a), $\theta = 30^\circ$; (b), $\theta = 90^\circ$.

4.3 Sound pressure level

The pressure spectra are now integrated from the Strouhal number $St = 0.15$ to provide the sound directivity. Figure 6 shows the computed sound pressure levels, with experimental data obtained by Mollo-Christensen *et al.*,¹³ Lush,¹⁴ and Stromberg *et al.*¹⁵ for jets with similar Mach numbers but various Reynolds numbers

The agreement between calculated and measured sound levels is very good for all observation angles. As expected, the acoustic level reaches a peak around an angle of $\theta = 30^\circ$. By considering the similarities between the noise radiated by jets with very different Reynolds numbers from 3600 up to 5.4×10^5 , the sound sources associated to the large scales seem to be relatively independent of the Reynolds number. Moreover, at high observation angles, the result of the simulation stands between the measurements which are relatively scattered. This behaviour can be associated to a Reynolds number effect, because the fine-scale turbulence is much less developed at low Reynolds numbers.

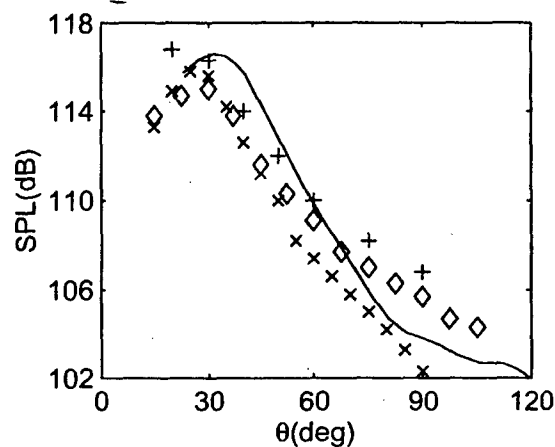


Figure 6: Sound pressure level as function of angle θ measured from the jet axis, at $60r_0$ from the jet nozzle. Experimental data by: +, Mollo-Christensen *et al.*¹³ ($M_j = 0.9$, $Re_D = 5.4 \times 10^5$); o, Lush¹⁴ ($M_j = 0.88$, $Re_D = 5 \times 10^5$); x, Stromberg *et al.*¹⁵ ($M_j = 0.9$, $Re_D = 3600$).

5. Conclusion

Results of a Large Eddy Simulation of a circular jet with a Mach number of 0.9 and a Reynolds number of 65000, carried out to compute directly the radiated sound field, has been presented. Both the flow field and the sound field computed have been investigated and compared systematically to experimental data available in the literature. Flow properties, namely flow development, mean flow parameters and turbulent intensities, are in very good agreement with measurements. The sound field provided by LES compares also successfully with experimental results in terms of directivity, spectra and levels. Sound sources in the jet are moreover found around the end of the potential core, as shown experimentally.

This study shows the feasibility of the direct calculation of the acoustic field generated by subsonic flows using LES. The excellent concordance with measurements supports that aerodynamic and acoustic mechanisms are well accounted for by the simulation. In that way, further works would have to investigate the generation mechanisms of jet noise.

Acknowledgments

Computing time is supplied by Institut du Développement et des Ressources en Informatique Scientifique (IDRIS - CNRS).

References

- ¹TAM, C.K.W., 1995, Computational aeroacoustics: issues and methods, *AIAA Journal*, **33**(10), 1788-1796.

- ²FREUND, J.B., LELE, S.K. & MOIN, P., 1998, Direct simulation of a Mach 1.92 jet and its sound field, *AIAA Paper* 98-2291.
- ³FREUND, J.B., 1999, Acoustic sources in a turbulent jet: a direct numerical simulation study, *AIAA Paper* 99-1858.
- ⁴MORRIS, P.J., LONG, L.N. & SCHEIDEGGER, T.E., 1999, Parallel computations of high speed jet noise, *AIAA Paper* 99-1873.
- ⁵SHEN, H. & TAM, C.K.W., 1998, Numerical simulation of the generation of the axisymmetric mode jet screech tones, *AIAA Journal*, **36**(10), 1801-1807.
- ⁶BOGEY, C., BAILLY, C. & JUVÉ, D., 2000, Numerical simulation of the sound generated by vortex pairing in a mixing layer, *AIAA Journal*, **38**(12), 2210-2218.
- ⁷TAM, C.K.W. & WEBB, J.C., 1993, Dispersion-relation-preserving finite difference schemes for computational acoustics, *J. Comput. Phys.*, **107**, 262-281.
- ⁸SMAGORINSKY, J.S., 1963, General circulation experiments with the primitive equations: I. the basic experiment, *Mon. Weath. Rev.*, **91**, 99-163.
- ⁹BOGEY, C., BAILLY, C. & JUVÉ, D., 2000, Computation of the sound radiated by a 3-D jet using Large Eddy Simulation, *AIAA Paper* 2000-2009.
- ¹⁰TAM, C.K.W. & DONG, Z., 1996, Radiation and outflow boundary conditions for direct computation of acoustic and flow disturbances in a nonuniform mean flow, *J. Comput. Acous.*, **4**(2), 175-201.
- ¹¹BOGEY, C., 2000, Calcul direct du bruit aérodynamique et validation de modèles acoustiques hybrides, Ph. D. Thesis of Ecole Centrale de Lyon, No. 2000-11.
- ¹²LAU, J.C., MORRIS, P.J. & FISHER, M.J., 1979, Measurements in subsonic and supersonic free jets using a laser velocimeter, *J. Fluid Mech.*, **93**(1), 1-27.
- ¹³MOLLO-CHRISTENSEN, E., KOLPIN, M.A. & MARTUCELLI, J.R., 1964, Experiments on jet flows and jet noise far-field spectra and directivity patterns, *J. Fluid Mech.*, **18**, 285-301.
- ¹⁴LUSH, P.A., 1971, Measurements of subsonic jet noise and comparison with theory, *J. Fluid Mech.*, **46**(3), 477-500.
- ¹⁵STROMBERG, J.L., MCLAUGHLIN, D.K. & TROUTT, T.R., 1980, Flow field and acoustic properties of a Mach number 0.9 jet at a low Reynolds number, *J. Sound Vib.*, **72**(2), 159-176.
- ¹⁶WYGNANSKI, I. & FIEDLER, H., 1969, Some measurements in the self-preserving jet, *J. Fluid Mech.*, **38**(3), 577-612.
- ¹⁷PANCHAPAKESAN, N.R. & LUMLEY, J.L., 1993, Turbulence measurements in axisymmetric jets of air and helium. Part I. Air jet. *J. Fluid Mech.*, **246**, 197-223.
- ¹⁸HUSSEIN, H.J., CAPP, S.P. & GEORGE, W.K., 1994, Velocity measurements in a high-Reynolds-number, momentum-conserving, axisymmetric, turbulent jet, *J. Fluid Mech.*, **258**, 31-75.

- ¹⁹BOERSMA, B.J., BRETHOUWER, G. & NIEUWSTADT, F.T.M., 1998, A numerical investigation on the effect of the inflow conditions on a self-similar region of a round jet, *Phys. Fluids*, **10**(4), 899-909.
- ²⁰RICOU, F.P. & SPALDING, D.B., 1961, Measurements of entrainment by axisymmetrical turbulent jets, *J. Fluid Mech.*, **11**, 21-32.
- ²¹CHU, W.T. & KAPLAN, R.E., 1976, Use of a spherical concave reflector for jet-noise-source distribution diagnosis, *J. Acoust. Soc. Am.*, **59**(6), 1268-1277.
- ²²JUVÉ, D., SUNYACH, M. & COMTE-BELLOT, G., 1980, Intermittency of the noise emission in subsonic cold jets, *J. Sound Vib.*, **71**(3), 319-332.